Publication Year	2018
Acceptance in OA	2020-10-07T14:28:55Z
Title	Unresolved Gamma-Ray Sky through its Angular Power Spectrum
Authors	Ackermann, M., Ajello, M., Baldini, L., Ballet, J., Barbiellini, G., Bastieri, D., Bellazzini, R., Bissaldi, E., Blandford, R. D., Bonino, R., Bottacini, E., Mizuno, T., Monzani, M. E., Morselli, A., Moskalenko, I. V., Negro, M., Nuss, E., ORIENTI, Monica, Orlando, E., Palatiello, M., Paliya, V. S., PERSIC, Massimo, Paneque, D., Pesce-Rollins, M., Petrosian, V., Piron, F., Porter, T. A., Principe, G., Rainò, S., Rando, R., Razzano, M., Razzaque, S., Reimer, O., Reimer, A., Serini, D., Sgrò, C., Siskind, E. J., Spandre, G., Spinelli, P., Suson, D. J., Tajima, H., Takahashi, M., Thayer, J. B., Torres, D. F., Tibaldo, L., Troja, E., Venters, T. M., Vianello, G., Wood, K., Yassine, M., Zaharijas, G., Ammazzalorso, S., Fornengo, N., Regis, M., Bregeon, J., Fermi-LAT Collaboration, Bruel, P., Buehler, R., Burns, E., Buson, S., Cameron, R. A., Caputo, R., CARAVEO, PATRIZIA, Cavazzuti, E., Chen, S., Chiaro, G., Ciprini, S., Costantin, D., Cuoco, A., Cutini, S., D'AMMANDO, FILIPPO, de la Torre Luque, P., de Palma, F., Desai, A., Digel, S. W., Di Lalla, N., Di Mauro, M., Di Venere, L., Fana Dirirsa, F., Favuzzi, C., Franckowiak, A., Fukazawa, Y., Funk, S., Fusco, P., Gargano, F., Gasparrini, D., Giglietto, N., Giordano, F., GIROLETTI, MARCELLO, Green, D., Grenier, I. A., Guillemot, L., Guiriec, S., Horan, D., Jóhannesson, G., Kuss, M., Larsson, S., Latronico, L., Li, J., Liodakis, I., Longo, F., Loparco, F., Lubrano, P., Magill, J. D., Maldera, S., Malyshev, D., Manfreda, A., Mazziotta, M. N., Mereu, I., Michelson, P. F., Mitthumsiri, W.
Publisher's version (DOI)	10.1103/PhysRevLett.121.241101
Handle	http://hdl.handle.net/20.500.12386/27659
Journal	PHYSICAL REVIEW LETTERS
Volume	121

Unresolved Gamma-Ray Sky through its Angular Power Spectrum

M. Ackermann,[1] M. Ajello,[2] L. Baldini,[5] J. Ballet,[6] G. Barbiellini,[7,8] D. Bastieri,[9,10] R. Bellazzini,[11] E. Bissaldi,[12,13] R. D. Blandford,[14] R. Bonino,[3,4] E. Bottacini,[14,15] J. Bregeon,[16] P. Bruel,[17] R. Buehler,[1] E. Burns,[18] S. Buson,[18] R. A. Cameron,[14] R. Caputo,[19] P. A. Caraveo,[20] E. Cavazzuti,[21] S. Chen,[9,15] G. Chiaro,[20] S. Ciprini,[22,23] D. Costantin,[10] A. Cuoco,[24,3] S. Cutini,[22,23] F. D'Ammando,[25,26] P. de la Torre Luque,[12] F. de Palma,[3] A. Desai,[2] S. W. Digel,[14] N. Di Lalla,[5] M. Di Mauro,[14] L. Di Venere,[12,13] F. Fana Dirirsa,[27] C. Favuzzi,[12,13] A. Franckowiak,[1] Y. Fukazawa,[28] S. Funk,[29] P. Fusco,[12,13] F. Gargano,[13] D. Gasparrini,[22,23] N. Giglietto,[12,13] F. Giordano,[12,13] M. Giroletti,[25] D. Green,[30,18] I. A. Grenier,[6] L. Guillemot,[31,32] S. Guiriec,[33,18] D. Horan,[17] G. Jóhannesson,[34,35] M. Kuss,[11] S. Larsson,[36,37] L. Latronico,[3] J. Li,[1] I. Liodakis,[14] F. Longo,[7,8] F. Loparco,[12,13] P. Lubrano,[23] J. D. Magill,[30] S. Maldera,[3] D. Malyshev,[29] A. Manfreda,[5] M. N. Mazziotta,[13] I. Mereu,[38] P. F. Michelson,[14] W. Mitthumsiri,[39] T. Mizuno,[40] M. E. Monzani,[14] A. Morselli,[41] I. V. Moskalenko,[14] M. Negro,[3,4,*] E. Nuss,[16] M. Orienti,[25] E. Orlando,[14] M. Palatiello,[7,8] V. S. Paliya,[2] D. Paneque,[42] M. Persic,[7,43] M. Pesce-Rollins,[11] V. Petrosian,[14] F. Piron,[16] T. A. Porter,[14] G. Principe,[29] S. Rainò,[12,13] R. Rando,[9,10] M. Razzano,[11] S. Razzaque,[27] A. Reimer,[44,14] O. Reimer,[44,14] D. Serini,[12] C. Sgrò,[11] E. J. Siskind,[45] G. Spandre,[11] P. Spinelli,[12,13] D. J. Suson,[46] H. Tajima,[47,14] M. Takahashi,[42] J. B. Thayer,[14] L. Tibaldo,[48] D. F. Torres,[49,50] E. Troja,[18,30] T. M. Venters,[18] G. Vianello,[14] K. Wood,[51] M. Yassine,[7,8] and G. Zaharijas[52,53]

(Fermi-LAT Collaboration)

S. Ammazzalorso,[3,4] N. Fornengo,[3,4] and M. Regis[3,4]

[1]*Deutsches Elektronen Synchrotron DESY, D-15738 Zeuthen, Germany*
[2]*Department of Physics and Astronomy, Clemson University, Kinard Lab of Physics, Clemson, South Carolina 29634-0978, USA*
[3]*Istituto Nazionale di Fisica Nucleare, Sezione di Torino, I-10125 Torino, Italy*
[4]*Dipartimento di Fisica, Università degli Studi di Torino, I-10125 Torino, Italy*
[5]*Università di Pisa and Istituto Nazionale di Fisica Nucleare, Sezione di Pisa, I-56127 Pisa, Italy*
[6]*Laboratoire AIM, CEA-IRFU/CNRS/Université Paris Diderot, Service d'Astrophysique, CEA Saclay, F-91191 Gif sur Yvette, France*
[7]*Istituto Nazionale di Fisica Nucleare, Sezione di Trieste, I-34127 Trieste, Italy*
[8]*Dipartimento di Fisica, Università di Trieste, I-34127 Trieste, Italy*
[9]*Istituto Nazionale di Fisica Nucleare, Sezione di Padova, I-35131 Padova, Italy*
[10]*Dipartimento di Fisica e Astronomia "G. Galilei", Università di Padova, I-35131 Padova, Italy*
[11]*Istituto Nazionale di Fisica Nucleare, Sezione di Pisa, I-56127 Pisa, Italy*
[12]*Dipartimento di Fisica "M. Merlin" dell'Università e del Politecnico di Bari, I-70126 Bari, Italy*
[13]*Istituto Nazionale di Fisica Nucleare, Sezione di Bari, I-70126 Bari, Italy*
[14]*W. W. Hansen Experimental Physics Laboratory, Kavli Institute for Particle Astrophysics and Cosmology, Department of Physics and SLAC National Accelerator Laboratory, Stanford University, Stanford, California 94305, USA*
[15]*Department of Physics and Astronomy, University of Padova, Vicolo Osservatorio 3, I-35122 Padova, Italy*
[16]*Laboratoire Univers et Particules de Montpellier, Université Montpellier, CNRS/IN2P3, F-34095 Montpellier, France*
[17]*Laboratoire Leprince-Ringuet, École polytechnique, CNRS/IN2P3, F-91128 Palaiseau, France*
[18]*NASA Goddard Space Flight Center, Greenbelt, Maryland 20771, USA*
[19]*Center for Research and Exploration in Space Science and Technology (CRESST) and NASA Goddard Space Flight Center, Greenbelt, Maryland 20771, USA*
[20]*INAF-Istituto di Astrofisica Spaziale e Fisica Cosmica Milano, via E. Bassini 15, I-20133 Milano, Italy*
[21]*Italian Space Agency, Via del Politecnico snc, 00133 Roma, Italy*
[22]*Space Science Data Center—Agenzia Spaziale Italiana, Via del Politecnico, snc, I-00133 Roma, Italy*
[23]*Istituto Nazionale di Fisica Nucleare, Sezione di Perugia, I-06123 Perugia, Italy*
[24]*RWTH Aachen University, Institute for Theoretical Particle Physics and Cosmology, (TTK), D-52056 Aachen, Germany*
[25]*INAF Istituto di Radioastronomia, I-40129 Bologna, Italy*
[26]*Dipartimento di Astronomia, Università di Bologna, I-40127 Bologna, Italy*
[27]*Department of Physics, University of Johannesburg, PO Box 524, Auckland Park 2006, South Africa*
[28]*Department of Physical Sciences, Hiroshima University, Higashi-Hiroshima, Hiroshima 739-8526, Japan*
[29]*Friedrich-Alexander-Universität Erlangen-Nürnberg, Erlangen Centre for Astroparticle Physics, Erwin-Rommel-Str. 1, 91058 Erlangen, Germany*
[30]*Department of Astronomy, University of Maryland, College Park, Maryland 20742, USA*
[31]*Laboratoire de Physique et Chimie de l'Environnement et de l'Espace—Université d'Orléans/CNRS, F-45071 Orléans Cedex 02, France*

[32]Station de radioastronomie de Nançay, Observatoire de Paris, CNRS/INSU, F-18330 Nançay, France
[33]The George Washington University, Department of Physics, 725 21st St, NW, Washington, DC 20052, USA
[34]Science Institute, University of Iceland, IS-107 Reykjavik, Iceland
[35]Nordita, Royal Institute of Technology and Stockholm University, Roslagstullsbacken 23, SE-106 91 Stockholm, Sweden
[36]Department of Physics, KTH Royal Institute of Technology, AlbaNova, SE-106 91 Stockholm, Sweden
[37]The Oskar Klein Centre for Cosmoparticle Physics, AlbaNova, SE-106 91 Stockholm, Sweden
[38]Dipartimento di Fisica, Università degli Studi di Perugia, I-06123 Perugia, Italy
[39]Department of Physics, Faculty of Science, Mahidol University, Bangkok 10400, Thailand
[40]Hiroshima Astrophysical Science Center, Hiroshima University, Higashi-Hiroshima, Hiroshima 739-8526, Japan
[41]Istituto Nazionale di Fisica Nucleare, Sezione di Roma "Tor Vergata", I-00133 Roma, Italy
[42]Max-Planck-Institut für Physik, D-80805 München, Germany
[43]Osservatorio Astronomico di Trieste, Istituto Nazionale di Astrofisica, I-34143 Trieste, Italy
[44]Institut für Astro- und Teilchenphysik and Institut für Theoretische Physik, Leopold-Franzens-Universität Innsbruck, A-6020 Innsbruck, Austria
[45]NYCB Real-Time Computing Inc., Lattingtown, New York 11560-1025, USA
[46]Purdue University Northwest, Hammond, Indiana 46323, USA
[47]Solar-Terrestrial Environment Laboratory, Nagoya University, Nagoya 464-8601, Japan
[48]IRAP, Université de Toulouse, CNRS, UPS, CNES, F-31028 Toulouse, France
[49]Institute of Space Sciences (CSICIEEC), Campus UAB, Carrer de Magrans s/n, E-08193 Barcelona, Spain
[50]Institució Catalana de Recerca i Estudis Avançats (ICREA), E-08010 Barcelona, Spain
[51]Praxis Inc., Alexandria, VA 22303, resident at Naval Research Laboratory, Washington, DC 20375, USA
[52]Istituto Nazionale di Fisica Nucleare, Sezione di Trieste, and Università di Trieste, I-34127 Trieste, Italy
[53]Center for Astrophysics and Cosmology, University of Nova Gorica, Nova Gorica 5000, Slovenia

(Received 6 July 2018; revised manuscript received 11 October 2018; published 12 December 2018)

The gamma-ray sky has been observed with unprecedented accuracy in the last decade by the *Fermi* - large area telescope (LAT), allowing us to resolve and understand the high-energy Universe. The nature of the remaining unresolved emission [unresolved gamma-ray background (UGRB)] below the LAT source detection threshold can be uncovered by characterizing the amplitude and angular scale of the UGRB fluctuation field. This Letter presents a measurement of the UGRB autocorrelation angular power spectrum based on eight years of Fermi-LAT Pass 8 data products. The analysis is designed to be robust against contamination from resolved sources and noise systematics. The sensitivity to subthreshold sources is greatly enhanced with respect to previous measurements. We find evidence (with $\sim 3.7\sigma$ significance) that the scenario in which two classes of sources contribute to the UGRB signal is favored over a single class. A double power law with exponential cutoff can explain the anisotropy energy spectrum well, with photon indices of the two populations being 2.55 ± 0.23 and 1.86 ± 0.15.

DOI: 10.1103/PhysRevLett.121.241101

Introduction.—The Universe has a network of structures. The so-called cosmic web was formed by gravitational instabilities, starting from the tiny density fluctuations that originated during primordial inflation, which evolved into structures at very different scales, from stars to galaxies, up to galaxy clusters and filaments. Furthermore, this texture nurtures the formation of nonthermal astronomical sources.

In ten years of operation, the *Fermi*-large area telescope (LAT) has been providing an unprecedented census of nonthermal emitters in gamma rays. The most recent Fermi-LAT eight-year preliminary point source list [FL8Y [1]] contains 5524 objects detected with a significance greater than 4σ between 100 MeV and 1 TeV.

Gamma-ray sources that are too dim to be resolved individually by Fermi-LAT contribute cumulatively to the unresolved gamma-ray background (UGRB); see Ref. [2] for a recent review. Although the exact composition of the UGRB is still an open issue, high-latitude sources are expected to be mostly of extragalactic origin. Therefore, they should follow the matter potential in the Universe (with some bias) and should be distributed anisotropically in the sky.

Different populations of gamma-ray emitters induce anisotropies in the UGRB with different amplitudes and different angular and energy spectra. A measurement of the gamma-ray angular power spectrum (APS) can therefore constrain the nature of the UGRB in a complementary way with respect to the intensity energy spectrum and the 1-point photon count probability distribution [3–8]. A different but related approach based on two-point statistics is the cross-correlation of the gamma-ray sky with independent probes tracing the large-scale structures of the Universe [9–25].

The first detection of anisotropies in the UGRB was reported by the Fermi-LAT Collaboration in 2012 [26], and then updated in 2016, employing 81 months of Pass 7 Fermi-LAT data from 0.5 to 500 GeV [27] (hereafter Fornasa *et al.*). The latter analysis revealed a hint that the

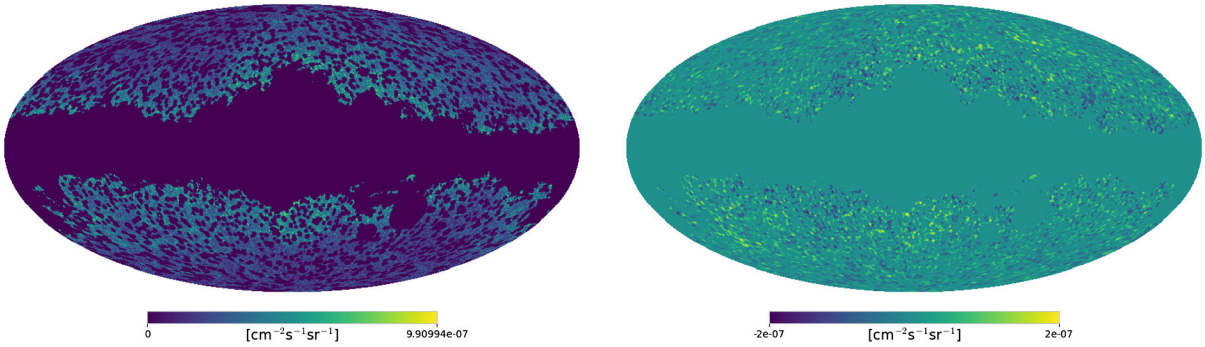

FIG. 1. Left: Mollweide projection of the all-sky intensity map for photon energies in the (1.7–2.8) GeV interval, after the application of the mask built for this specific energy bin; right: Mollweide projection of the UGRB map between (1.7–2.8) GeV. Masked pixels are set to 0; maps have been downgraded to order 7 for display purposes and smoothed with a Gaussian beam with $\sigma = 0.5°$ and $\sigma = 1°$, respectively.

measured APS might be due to more than one population of sources [28].

The raw APS (namely, the one that is measured directly from Fermi-LAT gamma-ray maps) is the sum of three contributions: (i) a noise term, C_N, due to fluctuations of photon counts, showing no correlation between different pixels in the sky and thus producing a flat APS; (ii) the autocorrelation of fluctuations due to individual sources with themselves (C_P): in the limit of point-like sources and infinite angular resolution of the telescope, this term shows up only at zero angular separation in real space (which implies a flat APS), but the finite size of the point-spread function (PSF) makes the associated APS decrease at high multipoles; (iii) the correlation between fluctuations induced by sources located in different positions in the sky: this contribution is expected to trace the cosmic web. C_N is expected to become less and less relevant as the statistics grow. C_P decreases as the brightest sources become resolved. In the current state of gamma-ray searches, it is still the dominant physical contribution to the APS. The third term is expected to eventually take over once the sensitivity of the telescope is such that a sufficiently large number of bright sources are resolved (and so no longer contribute to the UGRB).

Signal extraction.—A study of morphological anisotropies requires data with a good angular resolution. The data selection used in this analysis is designed to obtain the purest event sample and to maximize both the precision of the reconstructed arrival directions and the total photon counts statistics. For these reasons, we select Pass 8 [29] data of the P8R3_SOURCEVETO_V2 event class (the new SOURCEVETO event class, currently under development in the LAT collaboration and planned for public release, has an acceptance comparable to P8R2_CLEAN_V6 with a residual contamination almost equal to that of P8R2_ULTRACLEANVETO_V6 at all energies), and we reject the quartile of events with the worst PSF, which corresponds to all the events flagged as PSF0 type.

The data selection comprises eight years and is performed using version v10r0p5 of the Fermi Science Tools. Data in the energy range between 100 MeV and 1 TeV are subdivided into 100 logarithmically spaced "micro" bins, and for each of them we produce a count map and an exposure map, whose ratio gives 100 flux maps. They are then summed in order to obtain intensity maps in 12 "macro" energy bins between 524 MeV and 1 TeV (see Table I). This choice minimizes the effects of the energy dependence of the exposure, and we exploited this fine binning in the estimation of the autocorrelation as will be explained in the next section. Data are spatially binned with HEALPix [30] order 9.

The flux maps are masked such that the majority of the Galactic interstellar emission is removed, as well as the contribution from the resolved sources listed in the FL8Y source list [adding sources from the 3FHL catalog [31] when considering energies beyond 10 GeV]. The source mask is built taking into account both the brightness of each source and the energy dependence of the PSF. We tested the effectiveness of our masks performing several tests described in the Supplemental Material [32]. Figure 1 illustrates the mask built for the energy bin between 1.7 and 2.8 GeV.

In order to eliminate the residual Galactic contribution, we subtract the Galactic diffuse emission (GDE) with the model gll_iem_v6.fits described in Ref. [33]: in each micro energy bin, we perform a Poissonian maximum likelihood fit of data maps (considering only unmasked pixels) with the GDE model (with a free normalization) and a spatially constant term accounting for the UGRB and possible cosmic-ray residuals in the LAT; we find normalizations compatible with one within 1σ statistical uncertainty in each energy bin, and then we subtract the normalized GDE model from data maps. An example of masked map leaving only the UGRB in the energy bin (1.7–2.8) GeV is illustrated in the right panel of Fig. 1.

Angular power spectrum analysis.—The APS of intensity fluctuation is defined as $C_\ell^{ij} = (1/2\ell + 1)\langle \sum_m a_{\ell m}^i a_{\ell m}^{j*} \rangle$, where the brackets indicate the average on the modes m, the indexes i and j label the ith and the jth energy bins. When $i = j$, we refer to autocorrelation, to cross-correlation otherwise. The coefficients $a_{\ell m}$ are given by the expansion

in spherical harmonics of the intensity fluctuations, $\delta I_g(\vec{n}) = \sum_{\ell m} a_{\ell m} Y_{\ell m}(\vec{n})$, with $\delta I_g(\vec{n}) \equiv I_g(\vec{n}) - \langle I_g \rangle$ and $\vec{n}$ identifies the direction in the sky. The APS hence quantifies the amplitude of the anisotropy associated with each multipole ℓ, which roughly corresponds to a pattern "spot" size of $\lambda \simeq (180°/\ell)$.

We compute the APS with POLSPICE [36,37], a FORTRAN90 software tool which is based on the fast spherical harmonic transform. POLSPICE estimates the covariance matrix of the different multipoles taking into account the correlation effect induced by the mask with the algorithm described in [38,39]. Prior to the measurement, we exploited the standard HEALPix routine to remove the monopole and the dipole terms from the intensity maps in order to eliminate possible spectral leakage (owing to the masking) of these large-scale fluctuations (which have large amplitudes) on the small scales we are interested in.

The resolution of the maps and the effect of the PSF are accounted for respectively by the pixel window function, $W^{\rm pix}(\ell)$, and the beam window function, $W^{\rm beam}(E,\ell)$, whose computation is described in the SOM. Any random noise would contribute to the signal when the autocorrelation in the ith energy bin, $C_\ell \equiv C_\ell^{ii}$, is performed; hence it must be subtracted from the raw APS. We know that a Poissonian white noise would have a flat APS which can be estimated as in Fornasa *et al.*: $C_N = (\langle n^i_{\gamma,\rm pix}/(\epsilon^i_{\rm pix})^2 \rangle)/\Omega_{\rm pix}$, $n^i_{\gamma,\rm pix}$ being the photon counts in the unmasked pixels, $\epsilon^i_{\rm pix}$ the exposure, and $\Omega_{\rm pix}$ the pixel solid angle. Considering this as the only noise term, any other random component not following a Poisson distribution would not be taken into account. Moreover, the above equation for $\hat{C}_N$ represents only an estimator of the true C_N. Indeed, we found evidence of an underestimation of the noise term above a few GeV and devised a method to determine the autocorrelation APS without relying on the estimate of C_N. We exploit cross-correlations between different but closely adjacent micro energy bins: these are not affected by the noise term, because any kind of noise would not correlate between independent data samples. Also, we do not expect any effect due to the energy resolution of the instrument because the width of the micro bins is larger than the energy resolution, except for bins below 1 GeV (the first macro bin) whose result is anyway compatible with the one obtained by the standard autocorrelation method which is valid at those energies. As explained in the previous section, our macro energy bins are composed of a number N_b of micro energy bins. The APS computed in the macro bin can be seen as the sum of all the auto and cross APS computed for all the micro energy bins

$$C_\ell = \sum_{\alpha=1}^{N_b} C^{\alpha\alpha}_{\ell,\rm micro} + 2 \sum_{\substack{\alpha,\beta \\ \alpha>\beta}} C^{\alpha\beta}_{\ell,\rm micro}, \qquad (1)$$

where $\alpha, \beta = 1, \ldots, N_b$.

Under the reasonable assumption that the contributing sources have a broad and smooth energy spectrum, the APS for each macro energy bin can be obtained as

$$C_\ell = \frac{N_b}{N_b - 1} \sum_{\substack{\alpha,\beta \\ \alpha\neq\beta}} \frac{C^{\alpha\beta,\rm Pol}_{\ell,\rm micro}}{W_{E_\alpha}(\ell) W_{E_\beta}(\ell)}, \qquad (2)$$

where $W_{E_\alpha}(\ell) = W^{\rm beam}_{E_\alpha}(\ell) W^{\rm pix}_{E_\alpha}(\ell)$ and N_b is the number of micro bins in each macro energy bin [note that Eq. (2) returns a better approximation if the width of the micro bins decreases, and/or N_b increases, and/or the global spectrum of the underlying source population flattens. We calculated that when $N_b > 3$, considering our micro energy bin width and an anisotropy energy spectrum $\sim E^{-4}$, the difference between Eqs. (1) and (2) is less than 1%. We use $N_b = 6$ for all but the two highest-energy macro bins, for which we use $N_b = 11$ and $N_b = 12$, respectively.]. In this way, we avoid relying on the autocorrelation of the micro bins and therefore on the estimate of the noise. The SOM provides more details to support this approach.

Autocorrelation anisotropy energy spectrum.—For each energy bin, we find no evidence for an ℓ-dependent APS. This flat behavior is expected if the anisotropy signal is dominated by unresolved pointlike sources isotropically distributed in the sky. We therefore derive the level of anisotropy, C_P, for each energy bin by fitting the APS with a constant value: this provides the energy spectrum of the anisotropy signal due to gamma-ray pointlike sources. Prior to this fit, each APS was binned to reduce the correlation among neighboring C_ℓ. To carry out the binning in the most effective way, we implemented the unweighted averaging procedure proposed in Fornasa *et al.*, which was validated with Monte Carlo simulations (see Sec. IV-A of Fornasa *et al.*). The range of multipoles considered for the fitting

TABLE I. C_P values and the corresponding errors δC_P for each energy bin, as well as the range of multipoles considered in the fit of the APS and the systematic error associated to the instrumental effective area.

$E_{\rm min} - E_{\rm max}$ [GeV]	Fit range [$l_{\rm min}$-$l_{\rm max}$]	$C_P \pm \delta C_P$ [cm^{-4} s^{-2} sr^{-2} sr]	$C^{\rm sys}_{P,A_{\rm eff}}$ [%]
0.5–1.0	50–150	(3.7 ± 1.5) E-18	20
1.0–1.7	50–250	(6.6 ± 1.6) E-19	20
1.7–2.8	50–450	(9.4 ± 1.8) E-20	20
2.8–4.8	50–600	(3.4 ± 0.63) E-21	20
4.8–8.3	50–900	(1.4 ± 0.18) E-21	20
8.3–14.5	50–1000	(4.3 ± 0.61) E-22	20
14.5–22.9	50–1000	(9.0 ± 2.1) E-22	20
22.9–39.8	50–1000	(2.1 ± 1.0) E-22	20
39.8–69.2	50–1000	(5.9 ± 4.0) E-23	20
69.2–120.2	50–1000	(3.1 ± 1.5) E-23	22
120.2–331.1	50–1000	(1.2 ± 0.73) E-23	25
331.1–1000.0	50–1000	(-4.4 ± 11) E-25	32

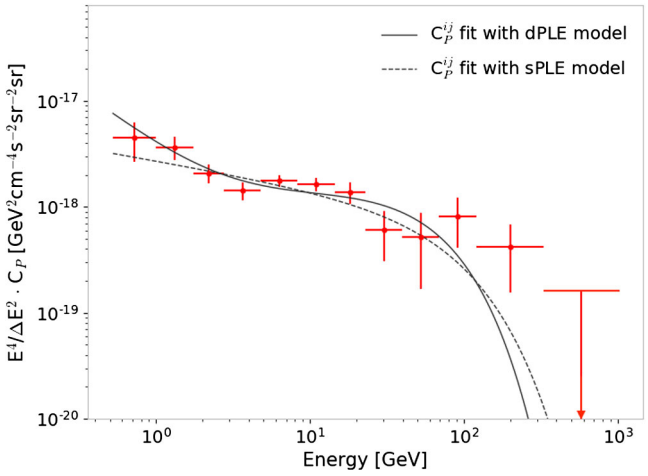

FIG. 2. Anisotropy energy spectrum $C_P(E)$, whose values are reported in Table I. We also show the best-fit models single power law with exponential cutoff (sPLE) and double power law with exponential cutoff (dPLE), and we stress that they have been obtained by considering the total set of C_P^{ij} from both auto- and cross-correlations between macro energy bins (see the last section for details about the fitting procedure).

procedure is determined taking into account several considerations: we exclude $l < 50$ where residual large-scale contributions from the foreground emission are significant and leakage from large-scale fluctuations still could be important; the beam window function correction is inaccurate when considering scales much smaller than the PSF: the upper limit in multipole depends on the PSF and on the photon statistics at a specific energy, and hence varies with the energy bin. Further details are provided in the SOM.

In Table I, we report the obtained C_P as a function of energy, as well as the fitting range of multipoles considered, and the systematics related to the uncertainty of the Fermi-LAT effective area $A_{\rm eff}$ [this uncertainty is obtained doubling the systematic uncertainty of the instrumental $A_{\rm eff}$, because the APS is the square of the intensity [40]].

Figure 2 shows our measurement of the anisotropy energy spectrum between 524 MeV and 1 TeV.

Cross-correlations between energy bins.—A way to discriminate whether the signal is due to either a single class or multiple classes of pointlike sources is to study the cross-correlations among energy bins: distinct populations of sources, presenting different energy spectra, reasonably lie in different sky positions.

Similarly, to the autocorrelation APS, we find flat cross-APS when performing cross-correlations between macro energy bins. If the anisotropy cross signal is due to a single class of sources, then $C_P^{ij} = \sqrt{C_P^{ii} C_P^{jj}}$, where C_P^{ii} and C_P^{jj} are the autocorrelation anisotropy levels in the energy bins i and j, respectively. The ratio $r_{ij} = C_P^{ij}/\sqrt{C_P^{ii} C_P^{jj}}$ is the cross-correlation coefficient: it should be compatible with 1 for each ij pair if the signal is due to a single class of sources. Figure 3 (left panel) shows the r_{ij} matrix: low-energy bins clearly correlate with nearby bins, while correlate less with the high-energy ones, and *vice versa*, meaning that sources contributing to the signal at low energy are not located at the same positions (on the spherical sky projection along the line of sight) as those that contribute at high energy. Hence, more than one class of source is present.

Discussion.—The global measurement, given by both the auto- and the cross-correlations, can be exploited to perform a statistical test, in order to establish whether a double-population scenario is favored with respect to a single-population case. We compute the χ^2 for two models: a single power law with an exponential cutoff (sPLE)

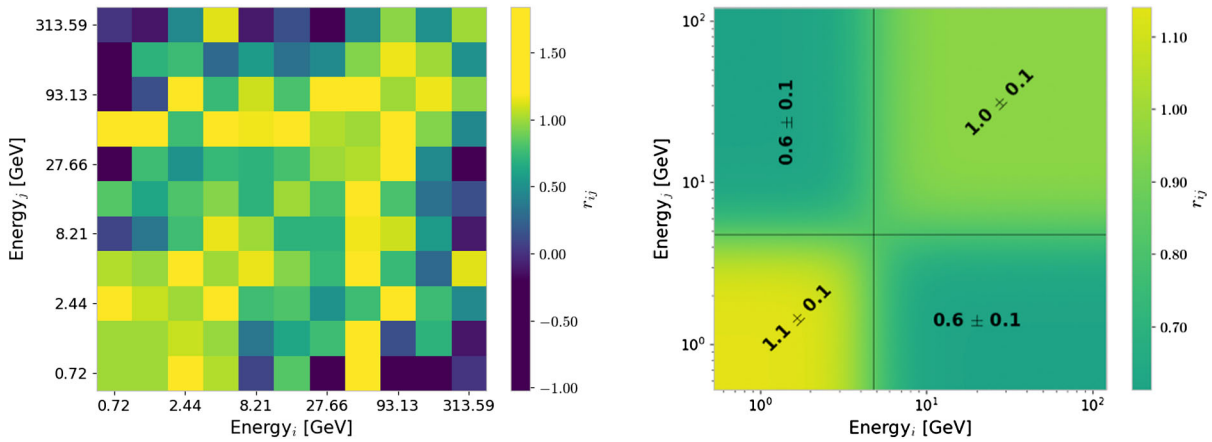

FIG. 3. Left: Cross-correlation coefficient r_{ij} matrix. This matrix is symmetric and has 1 on the diagonal by construction; the column and the row involving the last energy bin have been removed because the autocorrelation value is negative there and the corresponding r_{ij} values have negative roots. Right: mean values and standard deviation of the mean in each subrectangle of the r_{ij} matrix. If only one population contributed to the anisotropy signal, the mean values in the off-diagonal subrectangles would be values compatible with one, which is not the case.

TABLE II. Parameters of the fit of the global C_P^{ij} energy spectrum for both a single power law with an exponential cutoff and for a double power law with an exponential cutoff. $E_{\rm cut}$ is in GeV, whereas N_1 and N_2 have the same dimension as $E^2C_P^{ij}$. Degrees of freedom (DoF) is the difference between the number of C_P^{ij} considered $[12\times(12+1)]/2$ and the number of free parameters of the model. Because the fit has been performed on the C_P^{ij} normalized by a factor whose global dimension is E^2, a factor of 2 should be added to the indices of the power laws to obtain the values in terms of intensity spectra.

	Fit Parameters						
Model	N_1	α	N_2	β	$E_{\rm cut}$	χ^2	DoF
sPLE	(2.7 ± 0.3)E-18	0.13 ± 0.03	⋯	⋯	170 ± 50	84.7	75
dPLE	(3.5 ± 0.8)E-18	0.55 ± 0.23	(7.6 ± 6.4)E-19	-0.14 ± 0.15	89 ± 24	72.5	73

(3 free parameters: normalization, spectral index, and cutoff energy) and a double power law with an exponential cutoff (dPLE) (5 free parameters: 2 normalizations, 2 indexes, and the cutoff energy [for simplicity (i.e., to reduce the number of parameters) and because we expect the first population to be subdominant at high energy, we apply a single spectral cutoff]). The analytical expressions of these two models are

$$N_1\times(E_iE_j)^{-\alpha}e^{[-(E_i+E_j/E_{\rm cut})]} \quad (3)$$

$$[N_1\times(E_iE_j)^{-\alpha}+N_2\times(E_iE_j)^{-\beta}]e^{[-(E_i+E_j/E_{\rm cut})]}. \quad (4)$$

The fit is performed on the P_C^{ij} normalized by $E_i^2E_j^2/[(\Delta E_i)(\Delta E_j)]$, where E_i and E_j refer to the logarithmic center of the ith and jth energy bins, and the resulting best-fit parameters are summarized in Table II. The results of the best fits for the autocorrelation amplitudes C_P are shown in Fig. 2.

The chi-square difference between the two best-fit configurations is $\Delta\chi^2=\chi^2_{\rm sPLE}-\chi^2_{\rm dPLE}=12.24$. In order to obtain the statistical significance of the result, we performed 10^7 Monte Carlo samplings of the null hypothesis (the sPLE model) and derived the distribution of the chi-square differences, from which we determine a preference for the dPLE model at the 99.98% C.L. (corresponding to $\sim3.7\sigma$). Details about the Monte Carlo simulation can be found in the SOM.

The two power-law indices resulting from the best fit of the dPLE model are -2.55 ± 0.23, for the low-energy component, and -1.86 ± 0.15, for the one dominating above a few GeV.

The best fit for the dPLE model reveals a transition range between the two populations around 4 GeV. Separating the first four energy bins from the following six bins (we exclude the last two energy bins, which are completely beyond $E_{\rm cut}$, in order to avoid energies affected by absorption by the extragalactic background light), we define four subrectangles of the cross-correlation coefficient matrix, and evaluate the mean and the standard deviation of the mean for each subrectangle. The values are shown in the right-hand panel of Fig. 3: the off-diagonal region deviates from 1 at 4σ, which unequivocally favors a double population scenario.

Although detailed modeling of the underlying source classes is left for upcoming work, our findings are compatible with most of the contributions being from blazarlike sources above a few GeV. At lower energies, a population with a softer spectrum, such as possibly misaligned AGNs [41] or a different type of blazars [42], appears to dominate the UGRB.

The authors acknowledge Dr. Carlo Giunti for fruitful discussions about MC simulation procedures. The *Fermi*-LAT Collaboration acknowledges support for LAT development, operation, and data analysis from NASA and DOE (the United States), CEA/Irfu and IN2P3/CNRS (France), ASI and INFN (Italy), MEXT, KEK, and JAXA (Japan), and the K. A. Wallenberg Foundation, the Swedish Research Council, and the National Space Board (Sweden). Science analysis support in the operations phase from INAF (Italy) and CNES (France) is also gratefully acknowledged. This work performed in part under DOE Award No. DE-AC02-76SF00515. Some of the results in this Letter have been derived using the HEALPix package. This Letter is supported by the "Departments of Excellence" Grant awarded by the Italian Ministry of Education, University and Research (L. 232/2016). M. R. acknowledges support by the Excellent Young PI Grant "The Particle Dark-matter Quest in the Extragalactic Sky" funded by the University of Torino and Compagnia di San Paolo and by "Deciphering the high-energy sky via cross correlation" funded by Accordo Attuativo ASI-INAF n. 2017-14-H.0. N. F. acknowledges the research grant "The Anisotropic Dark Universe" No. CSTO161409, funded under the program CSP-UNITO "Research for the Territory" by Compagnia di Sanpaolo and University of Torino.

*Corresponding author.
michela.negro@to.infn.it

[1] https://fermi.gsfc.nasa.gov/ssc/data/access/lat/fl8y/.
[2] M. Fornasa and M. A. Sanchez-Conde, Phys. Rep. **598**, 1 (2015).
[3] H.-S. Zechlin, A. Cuoco, F. Donato, N. Fornengo, and M. Regis, Astrophys. J. Lett. **826**, L31 (2016).

[4] D. Malyshev and D. W. Hogg, Astrophys. J. **738**, 181 (2011).
[5] M. R. Feyereisen, S. Ando, and S. K. Lee, J. Cosmol. Astropart. Phys. 09 (2015) 027.
[6] H.-S. Zechlin, A. Cuoco, F. Donato, N. Fornengo, and A. Vittino, Astrophys. J. Suppl. Ser. **225**, 18 (2016).
[7] M. Lisanti, S. Mishra-Sharma, L. Necib, and B. R. Safdi, Astrophys. J. **832**, 117 (2016).
[8] M. Di Mauro, S. Manconi, H. S. Zechlin, M. Ajello, E. Charles, and F. Donato, Astrophys. J. **856**, 106 (2018).
[9] J.-Q. Xia, A. Cuoco, E. Branchini, M. Fornasa, and M. Viel, Mon. Not. R. Astron. Soc. **416**, 2247 (2011).
[10] S. Ando, A. Benoit-Lévy, and E. Komatsu, Phys. Rev. D **90**, 023514 (2014).
[11] J.-Q. Xia, A. Cuoco, E. Branchini, and M. Viel, Astrophys. J. Suppl. Ser. **217**, 15 (2015).
[12] M. Regis, J.-Q. Xia, A. Cuoco, E. Branchini, N. Fornengo, and M. Viel, Phys. Rev. Lett. **114**, 241301 (2015).
[13] A. Cuoco, J.-Q. Xia, M. Regis, E. Branchini, N. Fornengo, and M. Viel, Astrophys. J. Suppl. Ser. **221**, 29 (2015).
[14] S. Ando, J. Cosmol. Astropart. Phys. 10 (2014) 061.
[15] M. Shirasaki, S. Horiuchi, and N. Yoshida, Phys. Rev. D **92**, 123540 (2015).
[16] S. Ando and K. Ishiwata, J. Cosmol. Astropart. Phys. 06 (2016) 045.
[17] E. Branchini, S. Camera, A. Cuoco, N. Fornengo, M. Regis, M. Viel, and J.-Q. Xia, Astrophys. J. Suppl. Ser. **228**, 8 (2017).
[18] M. Lisanti, S. Mishra-Sharma, N. L. Rodd, and B. R. Safdi, Phys. Rev. Lett. **120**, 101101 (2018).
[19] M. Lisanti, S. Mishra-Sharma, N. L. Rodd, B. R. Safdi, and R. H. Wechsler, Phys. Rev. D **97**, 063005 (2018).
[20] S. Camera, M. Fornasa, N. Fornengo, and M. Regis, Astrophys. J. **771**, L5 (2013).
[21] S. Camera, M. Fornasa, N. Fornengo, and M. Regis, J. Cosmol. Astropart. Phys. 06 (2015) 029.
[22] M. Shirasaki, S. Horiuchi, and N. Yoshida, Phys. Rev. D **90**, 063502 (2014).
[23] M. Shirasaki, O. Macias, S. Horiuchi, S. Shirai, and N. Yoshida, Phys. Rev. D **94**, 063522 (2016).
[24] T. Tröster, S. Camera, M. Fornasa, M. Regis, L. van Waerbeke, J. Harnois-Déraps, S. Ando, M. Bilicki, T. Erben, N. Fornengo, C. Heymans, H. Hildebrandt, H. Hoekstra, K. Kuijken, and M. Viola, Mon. Not. R. Astron. Soc. **467**, 2706 (2017).
[25] N. Fornengo, L. Perotto, M. Regis, and S. Camera, Astrophys. J. **802**, L1 (2015).
[26] M. Ackermann, M. Ajello, A. Albert, L. Baldini, J. Ballet, G. Barbiellini, D. Bastieri *et al.* (Fermi-LAT Collaboration), Phys. Rev. D **85**, 083007 (2012).
[27] M. Fornasa, A. Cuoco, J. Zavala, J. M. Gaskins, M. A. Sánchez-Conde, G. Gomez-Vargas, E. Komatsu, T. Linden, F. Prada, F. Zandanel, and A. Morselli, Phys. Rev. D **94**, 123005 (2016).
[28] S. Ando, M. Fornasa, N. Fornengo, M. Regis, and Hannes-S. Zechlin, Phys. Rev. D **95**, 123006 (2017).
[29] https://fermi.gsfc.nasa.gov/ssc/data/analysis/documentation/Cicerone/Cicerone_Data/LAT_DP.html.
[30] K. M. Górski *et al.*, Astrophys. J.ApJ **622**, 759 (2005); http://healpix.sourceforge.net.
[31] M. Ajello *et al.* (Fermi-LAT Collaboration), Astrophys. J. Suppl. Ser. **232**, 18 (2017).
[32] See Supplemental Material at http://link.aps.org/supplemental/10.1103/PhysRevLett.121.241101 for further information about mask construction and foreground subtraction, window function computation, multipole range definition to derive the anisotropy level, estimation of the Poissonian noise, cross-check with the previous analysis, which includes Refs. [33–35].
[33] F. Acero *et al.* (Fermi-LAT Collaboration), Astrophys. J. Suppl. Ser. **223**, 26 (2016).
[34] M. Ackermann, M. Ajello, A. Albert *et al.* (Fermi-LAT Collaboration), Astrophys. J. **799**, 86 (2015).
[35] S. S. Wilks, Ann. Math. Stat. **9**, 60 (1938).
[36] I. Szapudi, S. Prunet, D. Pogosyan, A. S. Szalay, and J. R. Bond, Astrophys. J. Lett. **548**, L115 (2001).
[37] G. Chon, A. Challinor, S. Prunet, E. Hivon, and I. Szapudi, Mon. Not. R. Astron. Soc. **350**, 914 (2004).
[38] G. Efstathiou, Mon. Not. R. Astron. Soc. **349**, 603 (2004).
[39] A. Challinor and G. Chon, Mon. Not. R. Astron. Soc. **360**, 509 (2005).
[40] https://fermi.gsfc.nasa.gov/ssc/data/analysis/LAT_caveats.html.
[41] M. Di Mauro, F. Calore, F. Donato, M. Ajello, and L. Latronico, Astrophys. J. **780**, 161 (2014).
[42] M. Ajello, M. S. Shaw, R. W. Romani, C. D. Dermer, L. Costamante, O. G. King, W. Max-Moerbeck, A. Readhead, A. Reimer, J. L. Richards, and M. Stevenson, Astrophys. J. **751**, 108 (2012).